Experimental Investigation of Convergent Flow Disturbances for Performance Enhancement of Vertical-Axis Ocean Current Turbine at Low Current Speed in Indonesia

Madi Madi[1], Rahma Yanda[2], Meida Cahyo Untoro[3], Dendy Satrio[4], Tuswan Tuswan[5], Muhammad Gufran Nurendrawan Bangsa[1]

The ocean current speed in Indonesia is relatively low, but it has a huge ocean current energy potential, around 17.9 GW. However, this potential has not yet been optimally utilized in Indonesia. In this study, the influence of CoFD on the performance of Vertical-Axis Turbines (VAT) at low current velocities is investigated. Experimental methods were used to investigate the VAT without and with CoFD in a mini water tunnel. The investigation started with the distance between the flow disturbances and found that a distance of 0.75 times the diameter (0.75D) results in a maximum turbine power coefficient ($C_p max$) greater than 1 times the diameter (D), respectively 0.404 and 0.199. The self-starting capability was tested from 0 - 0.29 m/s, and at a minimum speed of 0.06 m/s, CoFD can increase the turbine rotation from 0 rpm (without CoFD) to 12.8 rpm (with CoFD 0.75D). Apart from that, CoFD (0.75D) is also able to increase the torque coefficient (C_t) of the turbine with a maximum value of 0.117 to 0.180 and the power coefficient (C_p) with a maximum value of 0.026 to 0.404. CoFD has therefore significantly enhanced VAT performance, especially at low current speeds, and is suitable for use in Indonesia.

KEYWORDS
~ Ocean current turbine
~ Low current speed
~ Flow disturbance
~ Vertical-axis turbines

[1] Institut Teknologi Sumatera, Energy System Engineering, South Lampung, Indonesia
[2] Institut Teknologi Sumatera, Integrated Water Management Engineering, South Lampung, Indonesia
[3] Institut Teknologi Sumatera, Informatics Engineering, South Lampung, Indonesia
[4] Institut Teknologi Sepuluh Nopember, Department of Ocean Engineering, Surabaya, Indonesia
[5] Universitas Diponegoro, Department of Naval Architecture, Semarang, Indonesia
e-mail: madi@tse.itera.ac.id
doi: 10.7225/toms.v14.n01.012

Received: 19 Aug 2024 / Revised: 16 Feb 2025 / Accepted: 16 Mar 2025 / Published: 20 Apr 2025

1. INTRODUCTION

Ocean currents are the movement of seawater masses caused by wind gusts, wave action, tides and density differences (Mukhtasor, 2014). The movement of ocean currents can generate kinetic energy, which scientists believe can be harnessed as a sustainable renewable energy source. Ocean currents also have an enormous density, which is up to 835 times higher than that of wind, just like ocean waves (Madi et al., 2022; Satrio et al., 2025). Ocean currents can therefore store enormous energy potential to meet the demand for electrical energy in coastal areas such as Indonesia.

The Indonesian Marine Energy Association has estimated the energy potential of ocean currents in Indonesia at 17.9 GW (Mukhtasor, 2014). The potential is very large considering that mapping has only been carried out at a few potential points in Indonesia's ocean areas. Apart from that, Indonesia has a large ocean that makes up 70% of its territory and has huge ocean energy sources, including ocean current energy (Purba et al., 2015). However, the enormous energy potential of ocean currents in Indonesia has yet to be optimally utilized. Furthermore, mapping conducted by the Indonesian Marine Energy Association shows that ocean current speeds in the Indonesian marine region are rather low, averaging less than 1 m/s (Satrio et al., 2022a). However, an average current velocity of more than 1 m/s is required to generate electrical energy (Satrio et al., 2022b). Therefore, it is a challenge for marine energy researchers in Indonesia to design ocean current power plant technology suitable for the conditions in Indonesian waters with low current velocities.

The commonly used ocean current power generation technology is a turbine to extract kinetic energy from ocean currents into mechanical energy (Madi et al., 2019). The most viable turbines for the study of low speed ocean currents are Vertical-Axis Turbines (VAT) (Zaidi et al., 2021; Yahya et al., 2023). The VAT also has the advantage of extracting the energy of the ocean current from different directions (Bachant & Wosnik, 2015; Akwa et al., 2012). However, the performance produced by VAT is still very low and causes little electrical energy generation (Satrio et al., 2016). Therefore, it is a challenge for ocean current turbine researchers to improve the performance of VAT at low current speeds.

Researchers have tried to improve the performance of VAT by modifying key turbine components such as foils, blades and rotors (Satrio, 2019). These three components are crucial parts of the turbine, so if they are modified, they will change their geometry, and their performance can change significantly, increasing or even decreasing it (Madi, 2020). The solution to improve the turbine performance without changing the crucial components has been carried out by researchers by adding external components of the turbine, such as an augmentation channel (Khan et al., 2008), an augmented diffuser (Mehmood et al., 2012), an open hydro (Belloni, 2013), a diffuser (Cresswell et al., 2015) and ducted artificial channel (Münch-Alligné et al., 2018). The result can improve the performance of the turbine, but it cannot accommodate current flow from the right and left sides due to the walls on both sides of the turbine (Khan et al., 2008; Mehmood et al., 2012; Belloni, 2013; Cresswell et al., 2015; Münch-Alligné et al., 2018). To overcome this problem, an experimental study was also conducted on the water flow deflector (plate guide vane) placed around the turbine rotor so that that ocean currents from all directions can be focused on the turbine rotor area, and the results improve the turbine performance. However, the problem of cavitation around the blade turbine arises, which leads to slight fatigue of the turbine (Madi et al., 2021a). In further experiments, the shape of the plate on the guide vane was changed to a foil, which has been shown to improve turbine performance and reduce cavitation (Madi et al., 2024a).

Flow disturbance is an external component of a turbine that has been empirically shown to significantly improve turbine performance at low current speed conditions (Satrio et al., 2022c; Satrio et al., 2024). The phenomenon of flow disturbance was first observed in an experimental investigation of a self-starting turbine in a towing tank operating at low current speeds. The experimental results indicated that circular flow disturbances generated turbulence that enabled enhanced turbine rotation (Satrio et al., 2021). The investigation of turbine performance in the presence of flow disturbances was initially conducted with numerical simulations employing Computational Fluid Dynamics (CFD). This study included a comparative analysis of the flow disturbances caused by NACA 63(4)021 and DU 06-W-200 hydrofoils under varying angles of attack (AoA). The numerical results demonstrated that both airfoils generate comparable power coefficients of 0.4622 and 0.4623 at 0.6 m/s flow velocity at 0 degrees angle of attack (Satrio et al., 2022b).

Subsequent numerical studies investigated the effects of circular cylindrical flow disturbances at angles of -60, 0 and 60 degrees. The findings indicated that these flow disturbances led to power coefficients of 0.190, 0.127 and 0.160, respectively, at a current speed of 0.50 m/s (Satrio et al., 2023a). Further studies on turbine performance optimization used numerical simulations to investigate variations in the diameter ratio of circular cylindrical flow disturbances. The results revealed that a diameter ratio of 0.5 at a current speed of 0.60 m/s led to a substantial performance enhancement, yielding a power coefficient of 0.442 (Satrio et al., 2023b). Further numerical analysis investigated the effects of varying the distance ratio of circular flow disturbances and showed that a distance ratio of 0 gave the highest performance with a power coefficient of 0.450 (Satrio et al., 2024). An experimental study was then conducted in an open channel using a NACA 63(4)021 hydrofoil as the flow disturbance mechanism. The results showed that a current speed of 0.180 was achieved at a flow velocity of 1 m/s (Madi et al., 2024b).

Ongoing research continues to explore strategies to improve performance, including the present study, which examines flow disturbance in water tunnels. The novelty of the current study lies in the implementation of a convergent NACA 0018 flow disturbance. In contrast to previous studies that focused on single flow disturbances, the present study introduces a convergent configuration that includes two flow disturbances (Table 1). This design is hypothesized to induce rotational effects within the flow field, thereby concentrating and accelerating the flow onto the turbine rotor, ultimately improving turbine performance.

References	Method	Flow Disturbance Shape	Number of Flow Disturbance	Current Speed (m/s)	$C_p max$
Satrio et al. (2022b)	Numeric (CFD)	Hydrofoil NACA 63(4)021 Hydrofoil DU 06-W-200	1	0.60	0.4622 0.4623
Satrio et al. (2023a)	Numeric (CFD)	Circular Cylinder (-60 degrees)	1	0.50	0.190
Satrio et al. (2023b)	Numeric (CFD)	Circular Cylinder (Diameter Ratio, ds/D = 0.5)	1	0.60	0.442
Satrio et al. (2024)	Numeric (CFD)	Circular Cylinder (Distance Ratio, x/D = 0)	1	0.60	0.450
Madi et al. (2024)	Experiment (Open Channel)	Hydrofoil NACA 63(4)021	1	1	0.180
Present Study	Experiment (Water Tunnel)	Convergent Hydrofoil NACA 0018	2	0.29	0.404

Table 1. State of the art for the effect of flow disturbance on turbine performance

2. RESEARCH METHODS

2.1. Design and Fabrications

The blade design is very important in a turbine as it is the most crucial component and affects the performance of the turbine (Madi et al., 2021b). The blade is the turbine component that first comes into direct contact with the fluid flow, so there will be changes in force along the blade area, affecting the hydrodynamic performance (Talukdar et al., 2018). Apart from this, the blade plays an important role in converting kinetic energy into mechanical energy, which is then transferred from the shaft to rotate and turn the generator to produce electrical energy (Madi et al., 2019). Based on that, parameters such as geometry, number of blades and hydrofoil type must be properly determined when designing the VAT. The parameters and specifications of the blade geometry of the VAT are listed in Table 2. The number of blade parameters chosen was four because it can achieve good stability, does not cause vibration and has been proven to achieve higher performance (Madi et al., 2021c). The hydrofoil type parameter chosen is NACA 0018 because it is capable of producing optimal turbine performance (Mohamed, 2012; Patel et al., 2017; Hantoro et al., 2011; Hantoro et al., 2018).

Parameters	Specifications
Number of blades (N)	4
Blade span (S)	0.2 m
Turbine diameter (D)	0.2 m
Number of arms	8
Shaft diameter (d)	0.008 m
Aspect ratio (AR)	1
Chord length (C)	0.052 m
Foil type	NACA 0018

Table 2. Turbine blade design specifications

The flow disturbance design must also be determined in this investigation, as it is the main object for increasing VAT performance. The geometric shape of the flow disturbance in this study is a hydrofoil, as it has been shown to perform better than circular shapes (Satrio et al., 2022c). Hydrofoils can also lead to flow separation and vortexing, which is very suitable for VAT operating locations (Alrayah et al., 2015; Utama et al., 2020). In this study, two flow disturbances are used to form a convergent geometry with an angle of attack of 30˚. By adjusting the angle of attack, angle will also separate the flow more significantly and concentrate the flow (Alrayah et al., 2015; Utama et al., 2020). The convergent shape is designed in such a way that the flow can be significantly more concentrated and a narrower area is formed because it is limited by the two walls of the flow disturbance. Based on the law of continuity, a narrowed area will create a higher flow velocity, so that the low current speed will become higher and a better VAT performance can be achieved. NACA 0018, the same material as the VAT foil blade, was chosen for the design of the flow disturbance in this study. The chord length and the height of the flow disturbance are 2C and 2S, respectively. The geometric design of the Convergent Flow Disturbance (CoFD) and the VAT used in this study are shown in Figure 1.

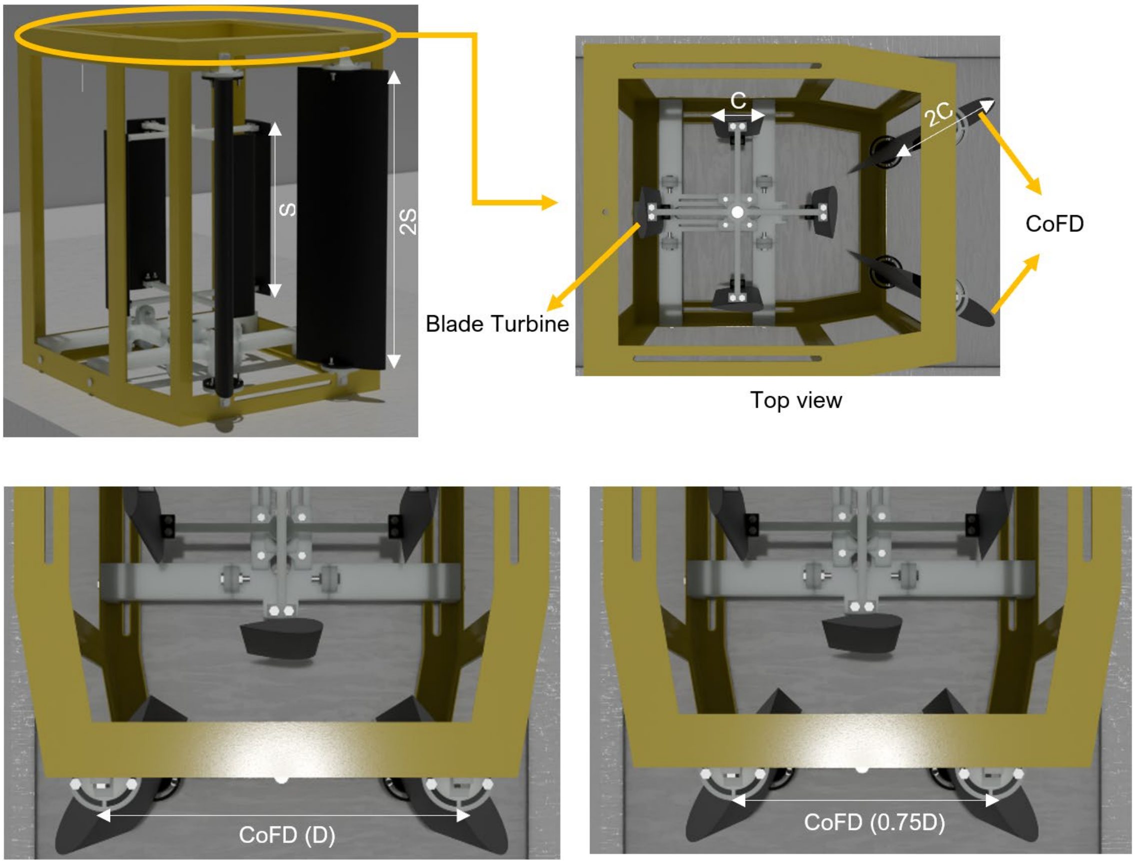

Figure 1. Turbine and CoFD design.

The turbine and CoFD production was carried out at the Energy Systems Engineering Laboratory, Institut Teknologi Sumatera. The main material used to make turbine blades and CoFDs is polylactic acid plus (PLA+) because it is more malleable, resistant to water, and can work very effectively with 3D printers (Mohammad et al., 2019), making it suitable for printing functional components such as small-scale prototypes. Turbine and CoFD manufacturing is done by printing the 3D model design results with a 3D printer. The individual parts of the printed turbine and CoFD are then assembled into a complete unit that can be tested as a prototype. The four blades are arranged vertically; each blade is connected to the upper and lower arms with two 50 mm M3 bolts and M3 nuts. The turbine arm is connected to the shaft via 14 mm bearings at the top and bottom. The material of the turbine shaft consists of carbon rods with a diameter of 0.008 m, while the supporting structure is made of iron that has been sprayed to protect against corrosion. The turbine shaft is connected to buffers attached to the top and bottom of the support structure so that the turbine forms a solid unit with the support structure. The CoFD is connected to a circular buffer with 15 mm M3 bolts and M3 nuts, and the circular buffer is connected to the support structure with 15 mm M5 bolts and M5 nuts, so that the CoFD can also be firmly connected to the support structure. The results of manufacturing the turbine, the CoFD and the support structure can be seen in Figure 2.

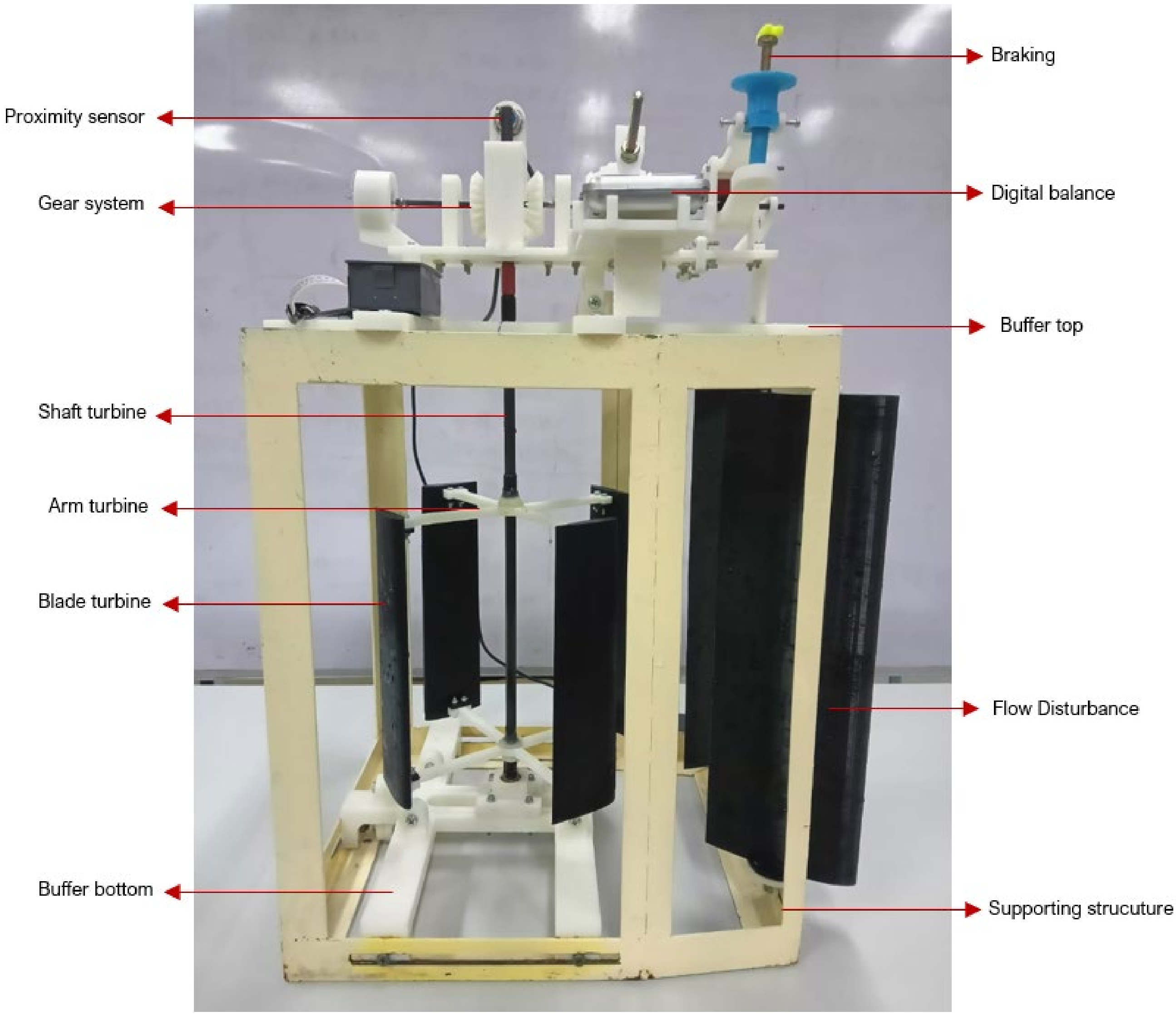

Figure 2. Turbine and CoFD fabricated

2.2. Experimental Setup and Apparatus

Turbine and CoFD studies were carried out experimentally in a mini water tunnel at the Energy Systems Engineering Laboratory, Institut Teknologi Sumatera. The detailed specifications of the water tunnel are listed in Table 3. The turbine and CoFD are permanently installed and held by a support structure to prevent them from shifting when exposed to the current flow. Figure 3 is a detailed illustration of the research object in the mini water tunnel under calm water conditions. The mini water tunnel can react to the movement of the water currents with the help of a water pump. The mini water tunnel is first filled with fresh water until the water level is high. Then the water pump draws water from the water outlet and pushes it towards the water inlet. The water flowing out of the water inlet continues to flow through the mini water tunnel and creates a water movement that can generate flow velocity and kinetic energy. The water will come out again through the water outlet with the suction of the water pump and the system will continue to operate repeatedly to create movement of water currents. The current speed is controlled by a dimmer that generates eight variations, namely 0.06 m/s, 0.09 m/s, 0.11 m/s, 0.13 m/s, 0.16 m/s, 0.20 m/s, 0.22 m/s and 0.29 m/s. The turbine is placed at 2D distance from the water inlet as this area produces the most stable water currents, and the turbine can work well based on the test results. The turbine works when the water inlet flows into the blade until it rotates. Then the turbine shaft transmits the rotation of the turbine to the gear system.

Parameters	Specifications
Length	1.2 m
Width	0.4 m
Depth	0.4 m
Draft	0.348 m
Velocity	0 – 0.29 m/s
Fluid temperature	27°C

Table 3. Mini water tunnel specifications

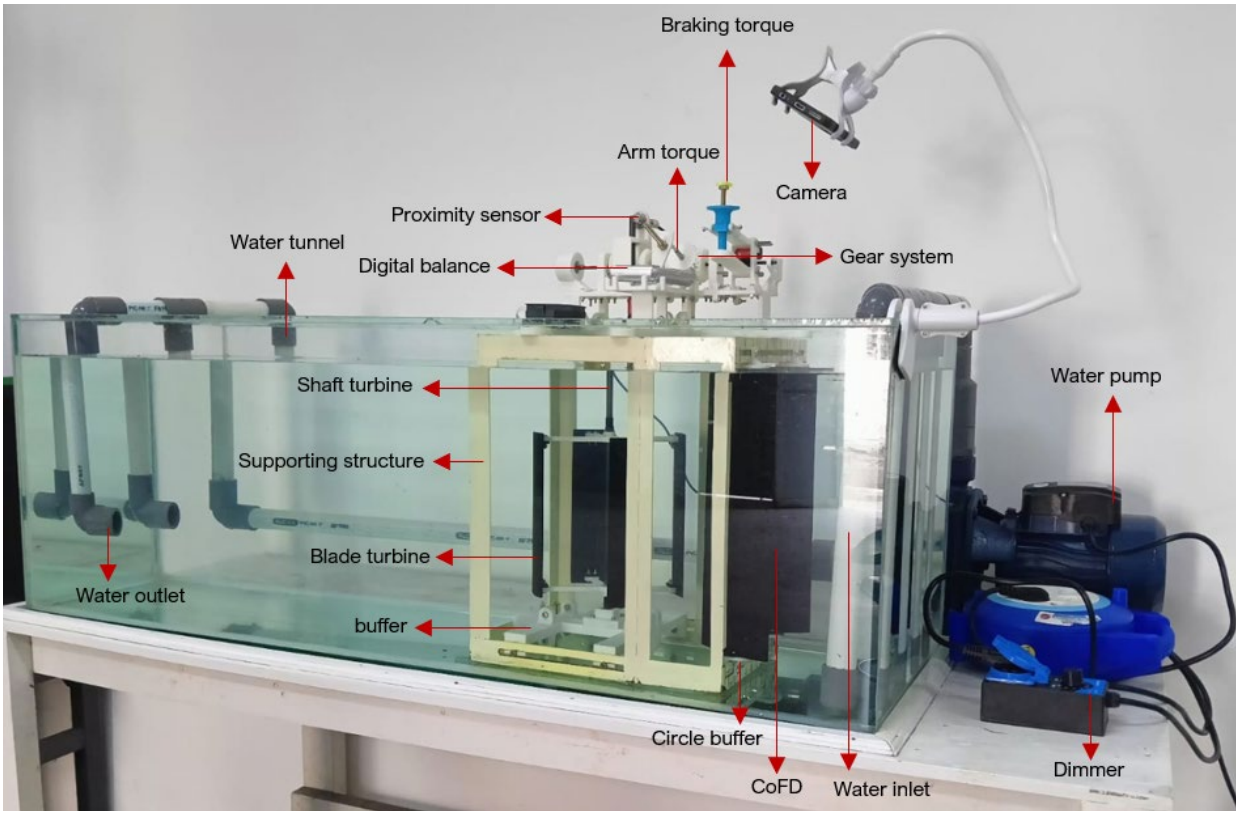

Figure 3. Experimental setup turbine with CoFD in water tunnel

In the present study, for the first time, variations of the distance between flow disturbances with a distance of D and 0.75D were investigated to obtain the best performance. After the best distance was determined, the self-starting capability of the turbine without CoFD and the turbine with the best distance CoFD are investigated. Then the torque and power coefficient of the turbine without CoFD and the turbine with the best distance CoFD were evaluated. The test variations consisted of: 1) the first test had two distance variations, and each variation tested six load braking to test performance, so there were 12 variations in the data collection; 2) the second test included two turbine variations (without and with best distance CoFD) and each turbine variation was tested with eight current speed variations to test self-start capability, so there were 16 variations in the data collection; and 3) the third test has two variations of the turbine (without and with CoFD best distance) and for each variation there are six load brakings to test performance, so there are 12 data collection variations. A total of 40 test variations were therefore carried out in this study.

Data collection on turbine rotation speed was performed using a proximity sensor calibrated with a tachometer in previous research (Figure 4), which gave an error of 3% (Madi et al., 2024a) and met the standards set by the International Towing Tank Conference (ITTC, 2017). The proximity sensor measures the turbine speed in units of revolutions per minute (rpm), which measures the self-starting capability of the turbine. Tip Speed Ratio (TSR) is a dimensionless number that represents the rotational speed of the turbine. TSR can be interpreted as the ratio of the circumferential speed (υ) to the current speed (V) in Equation 1. Omega (ω) is the angular velocity in 1/rad and nu (ν) is the rotational speed in 1/s or revolutions per minute (rpm) divided by 60 (Scholz, 2022).

$$TSR = \frac{v\,(R)}{V} = \frac{\omega R}{V} = \frac{2\pi\, v\, R}{V} \quad (1)$$

Where R is the radius of the turbine (m), and V is the current speed (m/s).

The turbine torque data is recorded using a digital balance that displays the turbine mass in grams. The digital balance has been calibrated with scale weights in previous studies (Figure 5) and no error was found (0 %) (Madi et al., 2024a). Calibration is performed by measuring one after the other of the seven weight scales (1, 2, 5, 10, 20, 50 and 100 grams) with a digital balance measuring instrument. The mass of the weight scales determined on the digital balance has the same value and the results are shown in the graph on the y-axis. The correlation value (R2) of the digital balance and the weight scale is equal to 1, which means that the regression line has perfect data or no error (0%). The results can also be seen in the graph that the y value is equal to x (y = x) or the correlation value (R2) is equal (Figure 5). The method of collecting turbine torque data utilizes the results of a patented dynamic torque sensor system where the rotation of the gear system is transmitted through the torque arm, which is then read by a digital balance so that the torque can be determined using Equation 2 (Hyte, 2014). The torque (T) can be represented by the torque coefficient (C_t) as shown in Equation 3.

$$T = M\,x\,g\,x\,r \quad (2)$$

$$C_t = \frac{T}{0.5\,p\,A\,V^2 R} \quad (3)$$

Where M is the mass of the load (kg) obtained from the digital balance, g is the acceleration due to gravity (9,8 m/s^2), r is the torque arm (m), p is density (998 kg/m^3), and A is the area of the turbine (m^2).

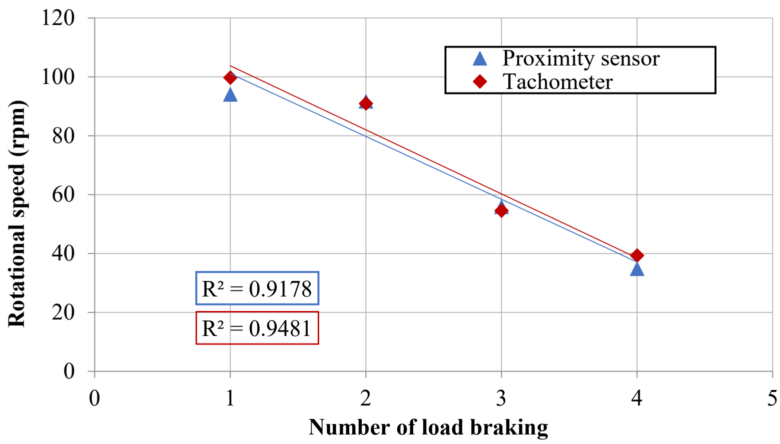

Figure 4. Calibration of the rotational speed ratio from the proximity sensor with a tachometer.

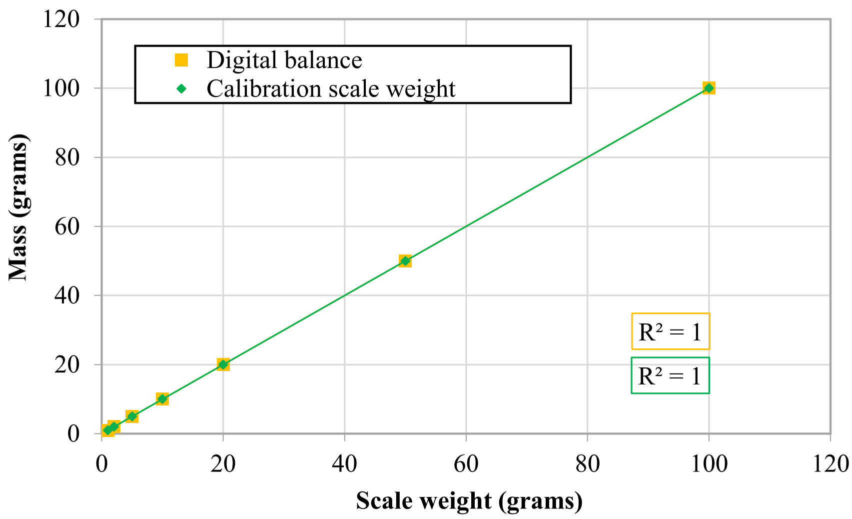

Figure 5. Calibration of the mass ratio as an indicator of torque from a digital balance with scale weight.

The data on torque and turbine speed were recorded at the same time as the turbine started up and recorded with a camera mounted above the research object. The turbine can be arranged in a variant to generate variations in the average speed and torque data by braking. Braking is a method of providing a torque load so that variations in the average torque and average rotational speed of the turbine can be obtained within a variation of the turbine. Stronger braking increases the torque load, but the turbine speed becomes slower. Braking is also required to determine the condition of the turbine that gives the best performance in a variation. In this study, the technique for regulating braking is performed by rotating the braking torque load. There are six braking variants (0˚, 360˚, 720˚, 1080˚, 1440˚, and 1800˚) where the first variant is not rotated, i.e. no load is applied, the second braking variant is rotated once (360˚), and the third to sixth variants are each extended by one revolution. The average torque and the turbine speed are determined from the mechanical power (P_t) according to Equation 4 and can be represented by the power coefficient (C_p) in Equation 5.

$$P_t = T\ \omega \tag{4}$$

$$C_p = \frac{P_t}{P_k} \tag{5}$$

P_k is the kinetic power of the water flow, calculated using Equation 6.

$$P_k = 0.5\ p\ A\ V^3 \tag{6}$$

3. RESULT AND DISCUSSION

3.1. Distance Between Flow Disturbance Experiments

The distance between the two flow disturbances was experimentally investigated, and the results of comparing 1 times the diameter (D) and 0.75 times the diameter (0.75D) were obtained. During the test, an experiment was also conducted with a distance of 0.5 times the diameter (0.5D), but the result was that the turbine could not rotate. In this case, varying the distance of the flow disturbance can increase or even affect the performance of the turbine. Legally, the continuity of the flow velocity is higher when the area is narrowed. This leads to the hypothesis that the smaller the flow disturbance distance, the narrower the area, so that the flow velocity is higher and the performance of the turbine increases. In this case, the water flow will be blocked, and it will be difficult to enter the rotor area of the turbine, so the turbine is difficult to work, as in the experimental results of the flow disturbance distance 0.5D. This incident is very interesting for this study as it investigates the distance between flow disturbances. Table 4 has the overall results of the CoFD distance comparison.

CoFD (D)		CoFD (0.75D)		CoFD (0.5D)	
C_p	TSR	C_p	TSR	C_p	TSR
0.008	2.321	0.023	2.887	0.000	0.000
0.116	2.389	0.132	2.741	0.000	0.000
0.158	2.335	0.318	2.618	0.000	0.000
0.192	2.309	0.313	2.495	0.000	0.000
0.186	2.255	0.389	2.446	0.000	0.000
0.199	2.234	0.404	2.305	0.000	0.000

Table 4. The CoFD distance comparison results

Figure 6 shows the relationship between the power coefficient C_p and the braking angle based on the variation in distance between the flow disturbances. The diagram shows the variation of the braking angle on the Vertical-Axis Turbine (VAT) with Convergent Flow Disturbance (CoFD) D and 0.75D. There are six variations of brake angles ranging from 0˚ to 1800˚ (0˚, 360˚, 720˚, 1080˚, 1440˚ and 1800˚). The diagram shows that the curve with the red diamond line (VAT with CoFD 0.75D) lies above the curve with the blue triangular line (VAT with CoFD D) in all braking fluctuation ranges. This means that VAT with CoFD (0.75D) achieved a better performance than VAT with CoFD (D). This is because the area between the CoFD at a distance of 0.75D is narrower than the distance D, which generates a higher current speed and the turbine power is higher. The highest power occurs at the sixth braking or an angle of 1800˚; this occurs because the turbine experiences a very large force from the braking load, so the resulting torque is enormous and causes the turbine to produce more power. The C_p CoFD (D) and CoFD (0.75D) at a braking angle of 1800˚ are 0.199 and 0.404 respectively, which means that CoFD (0.75D) can increase the VAT performance by 103% of CoFD (D). Conversely, the lowest performance occurs at the first braking or at an angle of 0˚; this happens because the turbine receives a very small force from the braking load, so the resulting torque is very small and the turbine works less. The C_p CoFD (D) and CoFD (0.75D) at a braking angle of 0˚ are 0.008 and 0.023 respectively, which means that CoFD (0.75D) can increase VAT performance by 187% compared to CoFD (D). The increase of C_p CoFD (0.75D) over CoFD (D) at the other four braking angles, namely 360˚, 720˚, 1080˚ and 1440˚, is 13.8%, 101%, 63% and 109%, respectively. Accordingly, the largest and smallest C_p increases occur at braking angles of 0˚ and 1080˚ respectively.

Figure 7 illustrates the visual flow event at the turbine during a convergent flow disturbance. Figure 7a explains the visual flow event when the VAT is given CoFD (D) with a flow velocity of 0.29 m/s is fed to the VAT. The observations in the image show that CoFD (D) has caused a flow separation and a slight concentration towards the turbine rotor, which is not too significant. Part of the flow has the same shape as the free stream velocity. At the same time, Figure 7b explains the visual flow event when the VAT CoFD (0.75D) is supplied at the same flow velocity. The observations in the image have shown that CoFD (0.75D) has caused a very clear flow separation, and most of it seems to be concentrated on the turbine rotor. The visual flow event in both images proves the truth about the performance of VAT with CoFD (0.75D), which can generate higher performance than VAT with CoFD (D). Accordingly, the addition of CoFD has a positive effect on the performance of VAT at a low current speed. In this study, the first test proved that the CoFD at a distance of 0.75D can produce better performance compared to the distance D. Therefore, the VAT with CoFD (0.75D) is compared with the VAT without CoFD (0.75D) to determine how much it affects the turbine performance (self-start, torque and power coefficient).

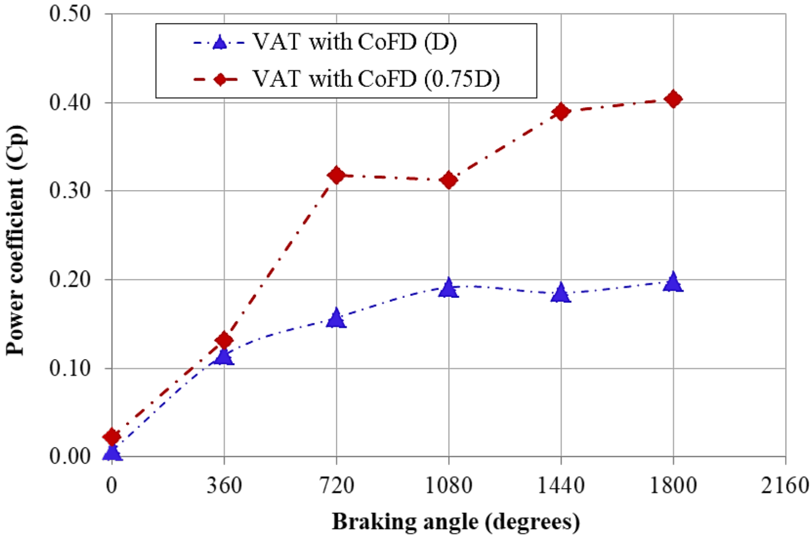

Figure 6. C_p- Braking angle curve of VAT with CoFD (D) and CoFD (0.75D).

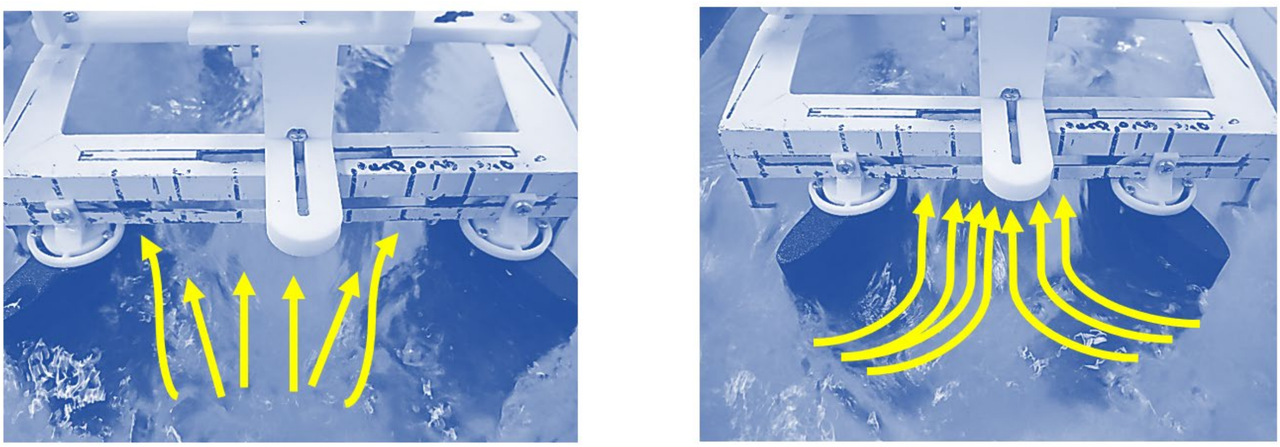

(a) (b)

Figure 7. Flow Visual 0.29 m/s (a) VAT with CoFD (D) and (b) VAT with CoFD (0.75D)

3.2. Self-Starting Capability Experiments

The best flow disturbance distance resulting from the investigations of the first test is 0.75D, which is then used as a benchmark for turbines without CoFD to determine the effects. In this second investigation, the ability of the turbine to start rotating without load was investigated, which is referred to as the self-starting capability of the turbine (Satrio & Utama, 2021; Madi et al., 2024a). The self-starting capability is measured when the input condition is the minimum current speed of the test turbine in the laboratory. In this study, a mini water tunnel with the lowest speed of 0.06 m/s was used as the test device. This is to determine the current speed required for the turbine to start working and generate electrical energy earlier. The self-starting test is measured when the turbine generates speed data in unit rotations per minute (rpm) at the minimum current speed. The value of the turbine rotational speed at the minimum speed will be very low because the hydrodynamic force on the turbine is very low. Therefore, the turbine can only generate a small amount of energy. If the current speed increases, the turbine receives an additional hydrodynamic force, which allows the turbine to absorb more energy, resulting in faster turbine rotation or a higher rpm value. Figure 8 shows the results of the turbine rotation speed without and with CoFD (0.75D) at a current speed of 0.29 m/s for 120 seconds. The diagram shows that the curve with the red diamond line (VAT with CoFD 0.75D) lies above the curve with the green rectangular line (VAT without CoFD 0.75D). This means that CoFD has significantly increased the value of the turbine speed and shows a slowly fluctuating curve for 120 seconds compared to VAT without CoFD. The highest value of turbine speed for VAT with and without CoFD (0.75D) is 84 rpm and 38 rpm respectively, which is an increase of 121%. The lowest value of the turbine rotation speed for VAT with and without CoFD (0.75D) is 78 rpm and 26 rpm respectively, which corresponds to an increase of 136%. The average value of the turbine rotation speed for VAT with and without CoFD (0.75D) is 81.2 rpm and 32.7 rpm respectively, which corresponds to an increase of 148 %. The test results of the turbine rotation speed at a maximum input current speed of 0.29 m/s show that CoFD (0.75D) can increase the rpm value, so that a better self-starting property is predicted.

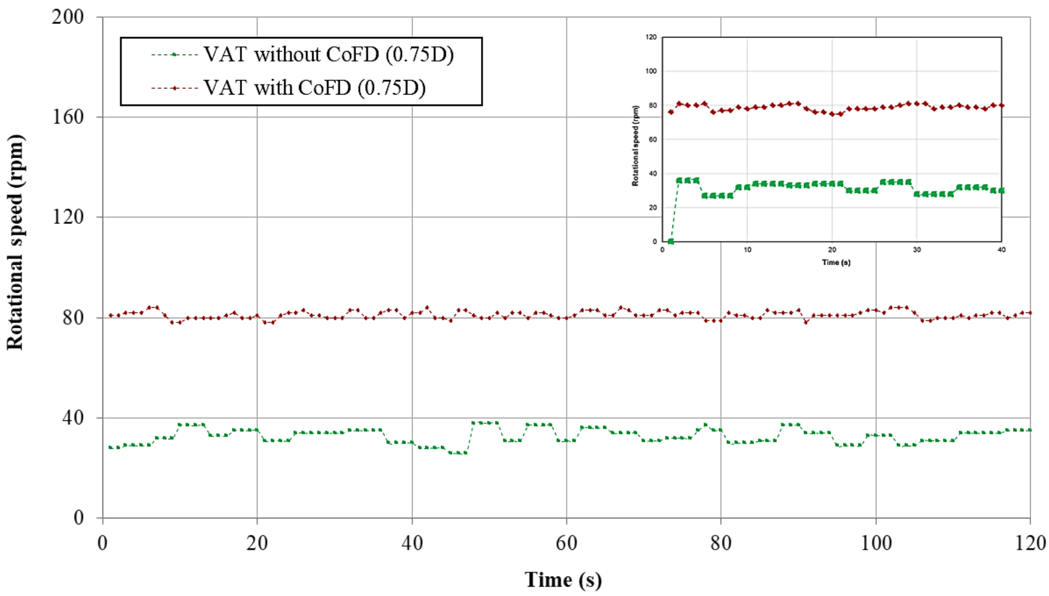

Figure 8. Time series on the rotational speed of VAT without and with CoFD (0.75D)

Figure 9 shows the relationship between variations in input current speed (x-axis) and the resulting turbine rotation speed (y-axis). The diagram shows that the red diamond line (VAT with CoFD 0.75D) lies above the green rectangular line (VAT without CoFD 0.75D) in all current speed ranges. Previously, it was also explained that CoFD could have a higher turbine rotation speed at a current speed of 0.29 m/s, which is the maximum input speed resulting from the mini water tunnel. When the input current speed is reduced and then reduced again to the point of minimum current speed, it also shows that CoFD can increase the value of turbine rotation speed. When the input current speed is reduced to 0.22 m/s, CoFD can increase the turbine rotation speed by 152% from 31.6 rpm to 79.6 rpm. When the input current speed is reduced to 0.20 m/s, 0.16 m/s, 0.13 m/s, 0.11 m/s and 0.09 m/s, CoFD can increase the turbine rotation speed by 157%, 153%, 128%, 116% and 237%, respectively. An interesting incident in this study was when the minimum current velocity input in the water tunnel showed that the turbine did not rotate; however, when CoFD (0.75D) was added, the turbine started to rotate. This event is referred to as the turbine's self-starting capability at minimum current speed.

In this study, the self-starting capability occurred at a current speed of 0.06 m/s when the turbine was provided with an additional CoFD (0.75D) with a rotation speed value of 12.8 rpm. The investigation began by performing a VAT test without CoFD (0.75D) at a current speed of 0.06 m/s. However, the turbine was unable to rotate. However, the turbine was unable to rotate or remain in position as shown by the 0 rpm speed data. This is because the hydrodynamic force on the turbine is very small and the kinetic power generated by the water flow is still very small at 0.004 watts. Therefore, the water power absorbed by the turbine is low and not sufficient to turn the turbine. However, when CoFD (0.75D) was added to the turbine at the same current speed, the results showed a turbine rotation speed value of 12.8 rpm. This is due to CoFD creating gaps with a narrow area and helping to direct the flow onto the turbine rotor, increasing the hydrodynamic force absorbed by the turbine and allowing the turbine to rotate. These results show that the self-starting ability of the turbine is excellent when the foil is changed to a flexible foil capable of rotating at 4 rpm at a current speed of 0.5 m/s (Sasmita et al., 2023); compared to changing the blade to an inclined blade capable of rotating at 2.25 rpm at a current speed of 0.2 m/s (Satrio & Utama, 2021); compared to changing the turbine rotor to a hybrid (darrieus-savonius) capable of rotating 1 rpm at a current speed of 0.2 m/s (Alam & Iqbal, 2010); and compared to adding a single flow disturbance capable of rotating 7.18 rpm at a flow speed of 0.4 m/s (Madi et al., 2024b). The test results of the self-starting capability of the turbine are also supported by the visual flow verification of VAT without and with CoFD (0.75D) at a minimum current speed of 0.06 m/s, as shown in Figure 10. VAT without CoFD 0.75D (Figure 10a) shows the same flow as the free stream; there is no visible flow separation and the flow in the turbine rotor area is very calm, indicating that the turbine is not rotating. VAT with CoFD 0.75D (Figure 10b) has the development of a slight turbulence in the area of the turbine rotor, marked with three yellow circles, indicating the rotation of the turbine.

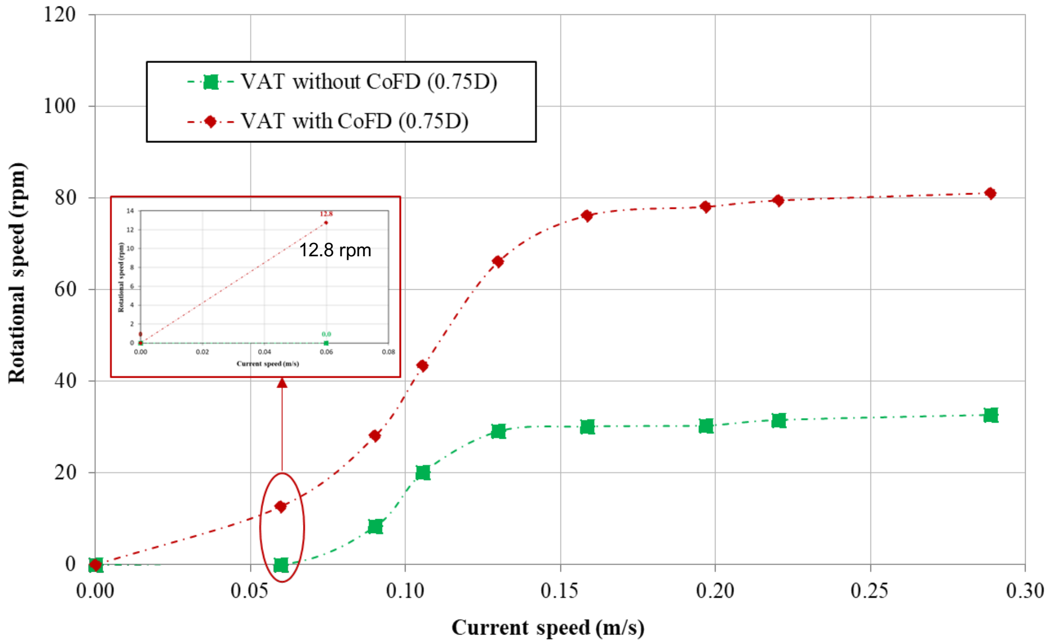

Figure 9. Self-starting capability of VAT without and with CoFD (0.75D)

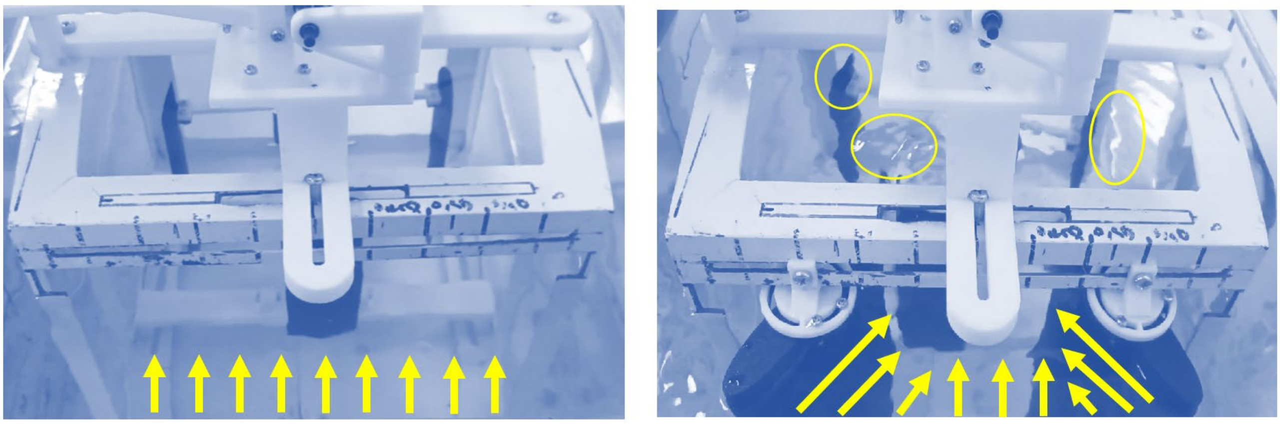

(a) (b)

Figure 10. Flow visual 0.06 m/s (a) VAT without CoFD (0.75D) and (b) VAT with CoFD (0.75D)

3.3. Torque Experiments

Figure 11 is a torque curve for 120 seconds at a braking angle of 1800˚ and a current speed of 0.29 m/s. The results have a significant difference in torque, with the curve with the red diamond (VAT with CoFD 0.75D) above the curve with the green rectangular line (VAT without CoFD 0.75D). This curve shows that CoFD 0.75D can increase the turbine torque at low current speeds. However, both curves show torque fluctuations, but the curve with the red diamond shows less fluctuation than the curve with the green rectangle, which tends to show more torque fluctuation. The fluctuating torque in a turbine is to be expected as the turbine continues to rotate through the upstream and downstream regions. The upstream region of the turbine extends from the first fluid flow that hits the blade face to the turbine shaft, while the downstream region extends from the turbine shaft to the rear blade (Sanvito et al., 2021). The blades in the upstream area will experience greater hydrodynamic forces as there is no prior disturbance, so they have greater torque.

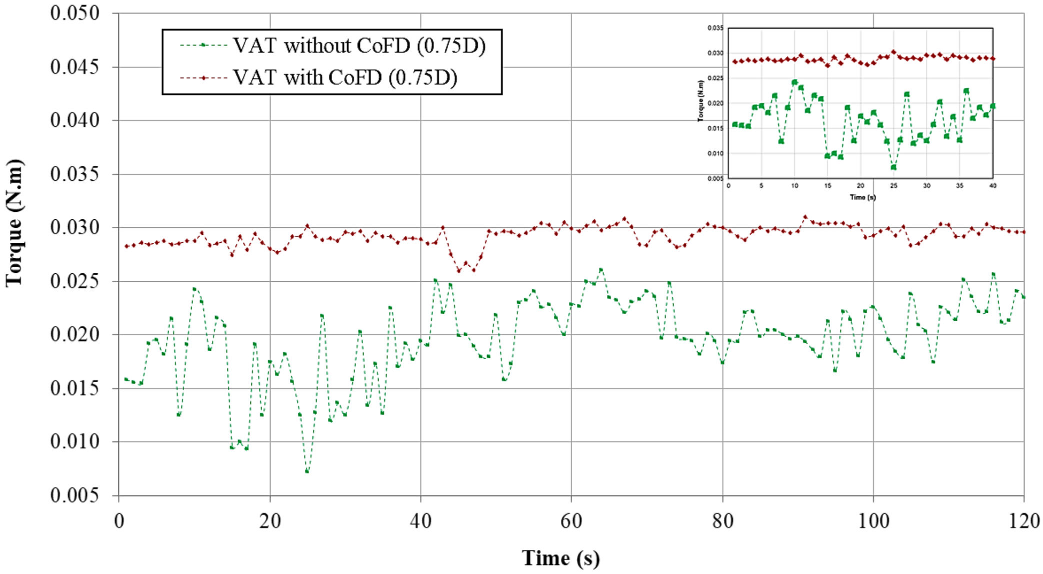

Figure 11. Time series on the torque of VAT without and with CoFD (0.75D).

Meanwhile, the blade experiences a small hydrodynamic force in the downstream area will because it has absorbed part of it in the upstream region, so that the resulting torque is lower. The difference between the torques in the upstream and downstream regions leads to fluctuations in the torque. The occurrence of large fluctuations is not good for the turbine itself, as it damages the turbine components (Shiono et al., 2002), causes vibration and fatigue in the turbine (Winchester & Quayle, 2011), so that the electrical power generation becomes unstable and the performance is no longer optimal. Therefore, the torque ripples need to be minimized so that the turbine components remain safe and have a long service life and the turbine performance is more stable and optimal.

The torque ripple factor (TRF) is a way to identify large and small torque fluctuations. The TRF can be determined by knowing the difference between the maximum torque value ($Tmax$) and the minimum torque ($Tmin$) or the difference between the maximum torque coefficient ($C_t max$) and the minimum torque coefficient ($C_t$min) during the test period with the turbine rotating (Marsh et al., 2015). Figure 12 shows the TRF results for all variations of the braking angle at VAT without and with CoFD (0.75D). The graph shows that the red diamond line (VAT with CoFD 0.75D) is below the green rectangular line (VAT without CoFD 0.75D). In addition, VAT with CoFD (0.75D) shows that the TRF value increases slightly parallel to the braking angle value.

In contrast, VAT without CoFD (0.75D) results in an unstable TRF value, that increases and decreases with increasing braking angle. This means that CoFD also has a positive effect on minimizing torque fluctuations, so that the turbine has a long service life because the turbine components are protected from vibration and fatigue. The turbine produces more stable and optimal energy. The minimum TRF values in VAT without and with CoFD (0.75D) occur at brake angles of 360˚ and 0˚ with TRF 0.003062 and 0.000417 respectively. The maximum TRF value for VAT without and with CoFD (0.75D) occurs at a braking angle of 1800˚ with TRF 0.018787 and 0.005010 respectively. Based on the maximum and minimum TRF values, it was shown that CoFD (0.75D) can lead to lower TRF values for the turbine.

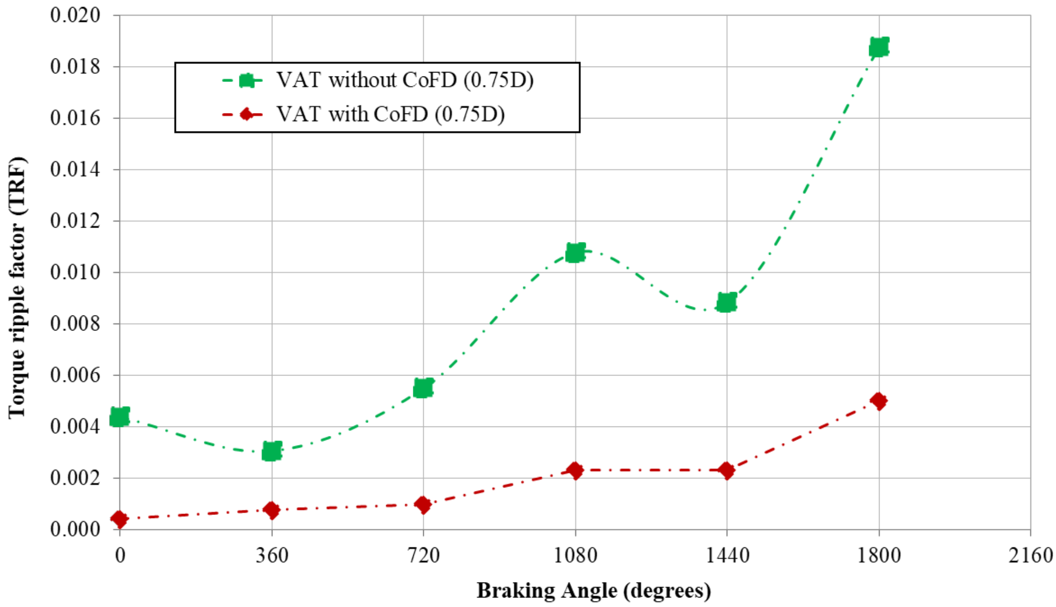

Figure 12. TRF – braking curve angle of VAT without and with CoFD (0.75D)

The torque can be expressed in dimensionless numbers, namely the torque coefficient (C_t), the ratio between the actual torque of the turbine resulting from the energy production and the theoretical torque according to Equation 3. Figure 13 compares C_t with the tip speed ratio (TSR) at VAT without and with CoFD (0.75D). *TSR* is a dimensionless number representing the current and turbine rotation speeds. The *TSR* value results from the ratio between the turbine rotation speed at the blade tip and the current speed, as shown in Equation 1. A large *TSR* value can represent a large value of current speed and turbine rotation speed and vice versa. The curve shows that the red diamond line (VAT with CoFD 0.75D) is higher and further away from the curve with the green rectangular line (VAT without CoFD 0.75D). The turbine position occupies a higher *TSR* when CoFD (0.75D) is added as the flow around the turbine rotor is accelerated, resulting in a higher turbine rotation speed.

The turbine without the addition of CoFD (0.75D), on the other hand, has a lower *TSR* value as there is no acceleration of the flow. Therefore, the turbine rotation speed is also low due to the low flow velocity in the mini water tunnel. The two curves also show that the larger the value of the turbine torque, the smaller the *TSR* value due to the braking factor. The larger the value of the given braking angle, the larger the turbine torque, but the turbine rotates slower; the same has been found in previous research (Talukdar et al., 2018; Madi et al., 2024a). The $C_t max$ value for VAT without and with CoFD (0.75D) occurs at *TSR* 0.22 and 2.30, respectively, with an increase of 49 %.

The $C_t min$ value for VAT without and with CoFD (0.75D) is at a *TSR* of 1.08 and 2.89 respectively, which corresponds to an increase of 60%. In this study, CoFD (0.75D) had a positive effect, as it can increase the turbine torque and reduce the TRF value. The addition of CoFD improves turbine performance without causing torque fluctuations, vibrations and fatigue, the turbine components are not easily damaged and the turbine has a long service life.

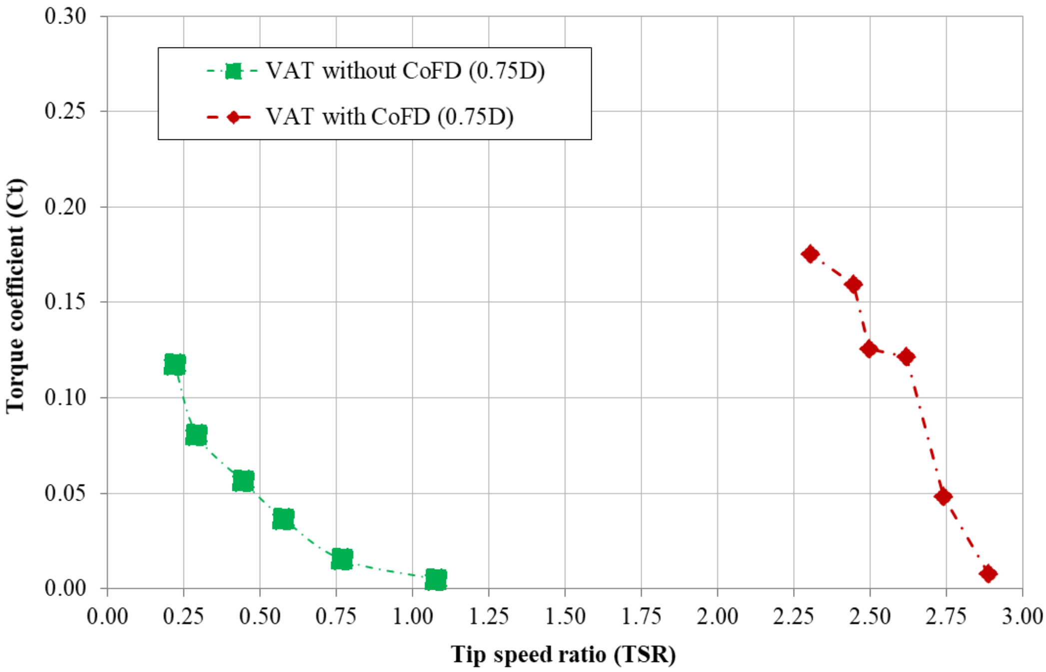

Figure 13. $C_t - TSR$ curve of VAT without and with CoFD (0.75D).

3.4. Power Coefficient Experiments

The power coefficient (C_p) is a dimensionless number that represents the mechanical power of the turbine (P_t). The C_p value is obtained from the turbine mechanical power (P_t) and the kinetic power of the flow (P_k), as shown in Equation 5. The mechanical turbine power is determined by multiplying the turbine torque (T) by the turbine rotation speed (ω), as explained in Equation 4. In simple terms, C_p can be interpreted as efficiency or the amount of fluid flow energy that the turbine absorbs to generate mechanical energy. Accordingly, the value of the mechanical turbine power is influenced by the torque and the turbine rotation speed. So, to obtain ample turbine mechanical power, it must have a high torque value and turbine rotation speed. However, to obtain ample torque, it is necessary to slow down the turbine rotation speed so it is necessary to adjust the turbine conditions to obtain torque and turbine speed values that can produce large C_p. Therefore, braking is one way that is needed to adjust the condition of the turbine. Figure 14 shows the relationship between C_p and the braking angle at VAT without and with CoFD (0.75D). The graph shows that the red diamond line curve(VAT with CoFD 0.75D) lies above the green rectangular line curve(VAT without CoFD 0.75D) along the brake angle variation, which means that CoFD (0.75D) can generate a higherC_p value. The condition of the turbine that can generate the highest C_p value occurs at a brake angle of 1800°, both for VAT without CoFD (0.75D) and with CoFD (0.75D) with C_p max values of 0.026 and 0.404 respectively.

The turbine condition with the lowest C_p value occurs at an angle of 0°, both for VAT without CoFD (0.75D) and with CoFD (0.75D) with $C_p min$ values of 0.005 and 0.023, respectively. This condition is comparable to the C_t results discussed previously, with $C_t min$ and $C_t max$, occurring at brake angles of 0° and 1800°, respectively. This means that these results confirm that large and small torque values can indicate large and small values of mechanical power generated by the turbine.

Turbines that are braked to different degrees can cause fluctuations in the turbine rotation speed. The more the turbine is braked, the slower its rotational speed becomes. Fluctuations in the deceleration of the turbine also lead to fluctuations in the rotational speed, so that the tip speed ratio (TSR) derived from Equation 1 can also vary. Figure 15 shows the relationship between C_p and TSR for VAT without and with CoFD (0.75D). The graph shows that the curve with the red diamond line (VAT with CoFD 0.75D) lies above the curve with the green rectangular line (VAT without CoFD 0.75D) and is higher. The graph also shows an enlargement of the green rectangular curve so that the pattern is clearly visible, and the pattern of the two curves is almost the same. The C_p value becomes higher for both VAT with CoFD (0.75D) and VAT without CoFD (0.75D) as the TSR decreases, and the same result is obtained for C_t - TSR. This is due to the braking factor; the more the turbine is braked, the higher the torque is, resulting in higher C_p and C_t values , but the rotation speed of the turbine becomes slower, resulting in a lower TSR. The resulting TSR of VAT without and with CoFD (0.75D) is 0.22 – 1.08 and 2.30 – 2.89 respectively, which means that the TSR of VAT without CoFD (0.75D) is lower because it produces a lower turbine rotation speed value than VAT with CoFD (0.75D). However, the TSR resulting from this study is still relatively low for both

VAT without CoFD (0.75D) and VAT with CoFD (0.75D), namely below three, because the input current speed in the mini water tunnel is also low, namely 0 – 0.29 m/s.

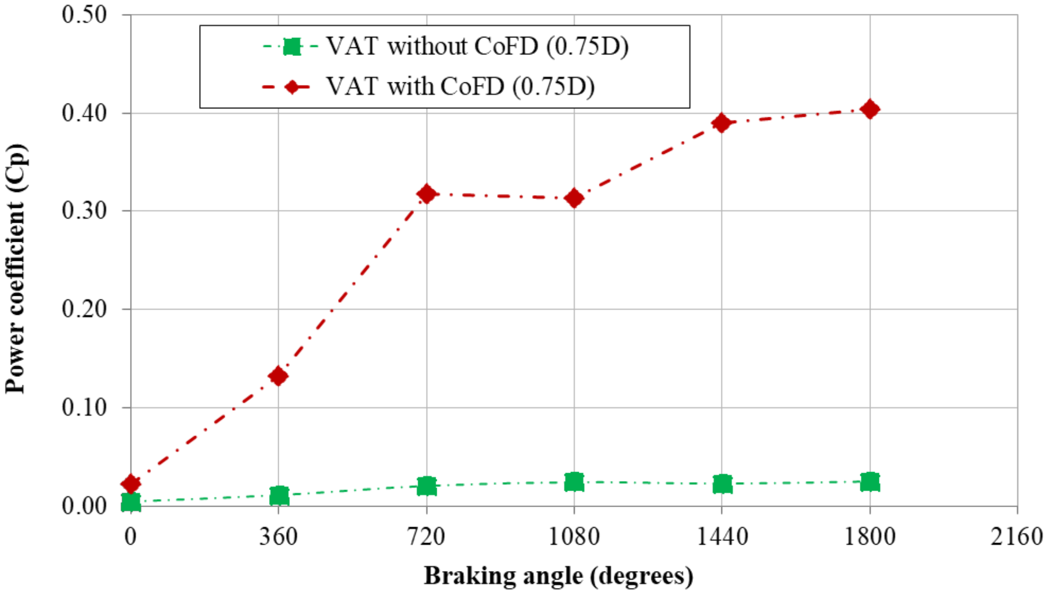

Figure 14. C_p – braking angle curve of VAT without and with CoFD (0.75D)

The two curves in this study directly show the $C_p max$ value without C_p events before the stall, which generally lead to C_p events in the stall and after the stall after the max value. The $C_p max$ value at VAT without and with CoFD (0.75D) shows a very large difference of 0.026 and 0.404, respectively. After the $C_p max$ value was visible on both curves, a C_p stall event occurred both at VAT without and with CoFD (0.75D), decreasing by 9% and 4% of the $C_p max$ value , respectively. This means that CoFD (0.75D) can also reduce the percentage of C_p stall values so that the difference in values is not too far from $C_p max$. C_p stall occurs because the turbine can no longer maintain the lift force, so that its performance decreases. The C_p, value after the stall shows that the C_p value at VAT without CoFD (0.75D) increased by 6 %, which means that the turbine can maintain the lift force again. The increase of C_p is due to the fact that the TSR value generated by VAT without CoFD (0.75D) is in a very low range, and generally a low TSR value can increase the lift force so that C_p can increase again. However, after that, VAT without CoFD (0.75D) experiences a continuous decrease of C_p with large percentages, namely 15%, 44% and 55%.

Meanwhile, C_p in VAT with CoFD (0.75D) decreased by 20 after stall, then increased again by 1%, after which C_p decreased by 58% and 83%, respectively. However, this study has shown that VAT with CoFD (0.75D) can generate a higher C_p value than VAT without CoFD (0.75D). The C_p value for VAT with CoFD (D) is still greater than VAT without CoFD. This means that CoFD has succeeded in making the turbine absorb more kinetic energy from the slow fluid flow, which can generate greater mechanical power. Therefore, CoFD is very suitable for use in Indonesian ocean areas to improve the performance of ocean current turbines so that more electrical energy can be generated to meet the electricity demand in Indonesia's coastal areas.

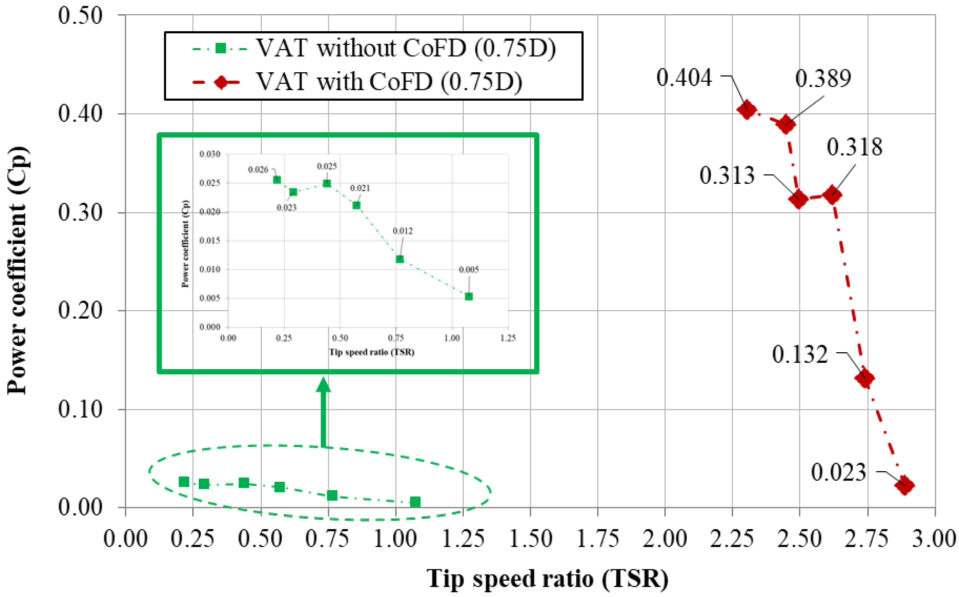

Figure 15. $C_p - TSR$ curve of VAT without and with CoFD (0.75D)

The findings of this study demonstrate that the implementation of a Convergent Flow Disturber (CoFD) effectively enhances the performance of a Vertical Axis Turbine (VAT) under low current speed conditions. Table 5 provides a summary of the performance outcomes for VAT both with and without CoFD.

Self-Starting Result			Torque Ripple Factor Result			Power Coefficient Result		
V (m/s)	without CoFD ω (rpm)	with CoFD ω (rpm)	Braking Angle (degrees)	without CoFD TRF	with CoFD TRF	Braking Angle (degrees)	without CoFD C_p	with CoFD C_p
0.000	0.00	0.00	0	0.0044	0.0004	0	0.005	0.023
0.060	0.00	12.77	360	0.0031	0.0008	360	0.012	0.132
0.090	8.37	28.20	720	0.0055	0.0010	720	0.021	0.318
0.106	20.14	43.42	1080	0.0108	0.0023	1080	0.025	0.313
0.130	29.11	66.25	1440	0.0088	0.0023	1440	0.023	0.389
0.159	30.17	76.31	1800	0.0188	0.0050	1800	0.026	0.404

Table 5. Summarizes the results of all performances VAT without and with CoFD

The first study, which focused on self-starting capability, shows that the presence of CoFD significantly increases the speed of the turbine from 0 rpm to 12.77 rpm at a current velocity of 0.06 m/s. This improvement is shown in green in Table 5. This improvement is highlighted in green in Table 5. The second investigation, in which the Torque Ripple Factor (TRF) was examined, shows that the VAT equipped with CoFD effectively reduces the torque fluctuations in all braking angle ranges. The lowest fluctuation is observed at a braking angle of 0 degrees, with a TRF value of 0.0004, as shown in green in Table 5. The third investigation, where the power coefficient was analyzed, shows that the power coefficient increases for VAT with CoFD across all braking angle ranges. The maximum power coefficient is measured at a braking angle of 1800 degrees and reaches a value of 0.404, which corresponds to an efficiency of 40.4 %; this result is also marked in green in Table 5.

4. CONCLUSION

Convergent Flow Disturbance (CoFD) was successfully and experimentally investigated in the Mini Water Tunnel, Energy Systems Engineering Laboratory, Institut Teknologi Sumatera. The test results show that CoFD can have a very significant positive impact, namely improving the Vertical-Axis Turbine (VAT) performance at low current speeds. Based on the results of the tests and analysis in this study, four conclusions were drawn;

1. The distance between the flow disturbance D and 0.75D was investigated, and the results show that CoFD (0.75D) performs better than CoFD (D). The $C_p max$ v values obtained with CoFD (D) and CoFD (0.75D) are 0.199 and 0.404, respectively, with an increase of 103% at a braking angle of 1800˚.
2. The investigation of the self-start capability of VAT without and with CoFD (0.75D) was conducted, and the results show that VAT with CoFD (0.75D) can increase the self-start capability at a minimum current speed of 0.06 m/s and a turbine rotation speed of 12.8 rpm is achieved. The the speed results increase with the increase of input current speed of 0.09 m/s, 0.11 m/s, 0.13 m/s, 0.16 m/s, 0.20 m/s, 0.22 m/s and 0.29 m/s with increases of 237%, 116%, 128%, 153%, 157%, 152% and 148%, respectively.
3. A study of the torque at VAT without and with CoFD (0.75D) was conducted, and the results show that VAT with CoFD (0.75D) can increase the torque with a more stable curve or little fluctuation. The TRF value at VAT with CoFD (0.75D) shows results that are smaller than all brake angle ranges, which means that the turbine fluctuations are small and the turbine does not fatigue easily. It does not vibrate easily, so the turbine components can last longer. Meanwhile, the C_t value for VAT with CoFD (0.75D) shows results larger than all braking angle ranges, which means that the torque from power generation has a larger value than VAT without CoFD (0.75D). The increase in the values of $C_t min$ and $C_t max$ after adding CoFD (0.75D) by the turbine was 60% and 49%, respectively.
4. The power coefficient (C_p) of VAT without and with CoFD (0.75D) was investigated. The results show that VAT with CoFD (0.75D) can significantly increase the C_p. This means that the turbine can generate a large mechanical power after being provided with CoFD (0.75D), so that it produces more electrical energy. The $C_p max$ values for VAT without and with CoFD (0.75D) are 0.026 and 0.404 respectively.

Based on the above four points, it can be concluded that CoFD can improve the VAT performance, i.e. self-starting, torque and power coefficient, at low current speed conditions. Therefore, CoFD is very suitable for use in Indonesian ocean areas with ocean current energy potential and low ocean current speed conditions. In the future, this research will be further developed in terms of sustainability to the implementation stage to meet the demand for electrical energy in Indonesian coastal areas. Further research work can be structured as follows. First, a numerical study using Computational Fluid Dynamics (CFD) for comparison will be conducted to ensure that the results of the present study can be validated. Then, a series of variation simulations will be conducted, including an investigation of the effects of immersion depth as studied by Ghamati et al. (2023), as well as variations in turbine blade geometry, such as the blade lift angle and the installation of winglets (Kariman et al., 2023). In addition, new blade shapes (Mohamed, 2012) and tubercle blade designs (Utama et al., 2020) are being investigated to determine the optimal blade geometry. After completing the simulations of the rotor blades, the results will be tested experimentally in a wind tunnel to obtain more accurate and validated results, following the approach of Hoseinzadeh et al. (2020). Next, the research will continue in a wave tunnel to comprehensively study the turbine and flow disturbances to ensure that its performance matches the experimental flow characteristics, as shown by Satrio et al. (2021). Subsequently, the research will be extended to open channels to evaluate the performance under environmental conditions, as conducted by Talukdar et al. (2018). In addition, the study will move to open sea testing in Indonesian waters to evaluate real-world environmental conditions, as done by Nugraha et al. (2018). Upon successful completion of these phases, the results are expected to contribute to the commercialization and implementation of this technology in Indonesia and ultimately help meet the electricity needs of coastal communities.

ACKNOWLEDGEMENT

The author would like to thank the Directorate General of Science, Technology and Higher Education Resources. The Ministry of Research, Technology and Higher Education of the Republic of Indonesia funds the current project with a scheme called Basic Research "Fundamental Research 2024" based on contract number 1570ay/IT9.2.1/PT.01.03/2024.

CONFLICT OF INTEREST

The authors have no conflicts of interest.

REFERENCES

Akwa, J.V., Vielmo, H.A. and Petry, A.P. (2012) 'A review on the performance of Savonius wind turbines', Renewable and Sustainable Energy Reviews, 16(5), pp. 3054–3064. Available at: https://doi.org/10.1016/j.rser.2012.02.056

Alam, M.J. and Iqbal, M.T. (2010) 'A low cut-in speed marine current turbine', The Journal of Ocean Technology, 5(4), pp. 49–61.

Alrayah, A. and Elseory, A.M. (2015) 'Numerical study on the effect of different backward step configurations on the aerodynamics performance of NACA 23012', in Int Conf Adv Mech Eng Istanbul, pp. 1–5.

Alsoufi, M.S., Alhazmi, M.W., Suker, D.K., Alghamdi, T.A., Sabbagh, R.A., Felemban, M.A. and Bazuhair, F.K. (2019) 'Experimental characterization of the influence of nozzle temperature in FDM 3D printed pure PLA and advanced PLA+', American Journal of Mechanical Engineering, 7(2), pp. 45–60. Available at: https://doi.org/10.12691/ajme-7-2-1

Bachant, P. and Wosnik, M. (2015) 'Performance measurements of cylindrical-and spherical-helical cross-flow marine hydrokinetic turbines, with estimates of exergy efficiency', Renewable Energy, 74, pp. 318–325. Available at: https://doi.org/10.1016/j.renene.2014.07.049

Belloni, C.S. (2013) Hydrodynamics of ducted and open-centre tidal turbines (Doctoral dissertation). University of Oxford. Available at: https://ora.ox.ac.uk/objects/uuid:0721090a-d8b1-45f8-a47b-45d9cdc47222

Cresswell, N.W., Ingram, G.L. and Dominy, R.G. (2015) 'The impact of diffuser augmentation on a tidal stream turbine', Ocean Engineering, 108, pp. 155–163. Available at: https://doi.org/10.1016/j.oceaneng.2015.07.033

Ghamati, E., Kariman, H. and Hoseinzadeh, S. (2023) 'Experimental and computational fluid dynamic study of water flow and submerged depth effects on a tidal turbine performance', Water, 15(13), p. 2312. Available at: https://doi.org/10.3390/w15132312

Hantoro, R., Utama, I.K.A.P., Erwandi, E. and Sulisetyono, A. (2011) 'An experimental investigation of passive variable-pitch vertical-axis ocean current turbine', Journal of Engineering and Technological Sciences, 43(1), pp. 27–40. Available at: https://doi.org/10.5614/itbj.eng.sci.2011.43.1.3

Hantoro, R., Utama, I.K.A.P., Arief, I.S., Ismail, A. and Manggala, S.W. (2018) 'Innovation in vertical axis hydrokinetic turbine–straight blade cascaded (VAHT-SBC) design and testing for low current speed power generation', Journal of Physics: Conference Series, 1022(1), 012023. Available at: https://doi.org/10.1088/1742-6596/1022/1/012023

Hoseinzadeh, S., Bahrami, A., Mirhosseini, S.M., Sohani, A. and Heyns, S. (2020) 'A detailed experimental airfoil performance investigation using an equipped wind tunnel', Flow Measurement and Instrumentation, 72, p. 101717. Available at: https://doi.org/10.1016/j.flowmeasinst.2020.101717

Hyte, J.R.A. (2014) Dynamic Torque Sensing System. United States Patent US 8,752,439 B2. Available at: https://patents.google.com/patent/US8752439B2/en?oq=US+8%2c752%2c439+B2

ITTC (2017) Uncertainty Analysis, Instrument Calibration.

Kariman, H., Hoseinzadeh, S., Khiadani, M. and Nazarieh, M. (2023) '3D-CFD analysing of tidal Hunter turbine to enhance the power coefficient by changing the stroke angle of blades and incorporation of winglets', Ocean Engineering, 287, p. 115713. Available at: https://doi.org/10.1016/j.oceaneng.2023.115713

Khan, M.J., Iqbal, M.T. and Quaicoe, J.E. (2008) 'River current energy conversion systems: Progress, prospects and challenges', Renewable and Sustainable Energy Reviews, 12(8), pp. 2177–2193. Available at: https://doi.org/10.1016/j.rser.2007.04.016

Madi, M., Mukhtasor, M., Satrio, D., Tuswan, T., Ismail, A., Rafi, R., Yunesti, P., Wira Buana, S. and Jarwinda, J. (2024a) 'Experimental Study on the Effect of Foil Guide Vane on the Performance of a Straight-Blade Vertical Axis Ocean Current Turbine', NAŠE MORE: znanstveni časopis za more i pomorstvo, 71(1), pp. 1–11. Available at: https://doi.org/10.17818/NM/2024/1.1

Madi, M., Mukhtasor, M., Walujo Prastianto, R., Tuswan, T. and Ismail, A. (2022) 'Experimental study on the effect of arm design on the performance of a flap-float horizontal ocean wave energy converter', NAŠE MORE: znanstveni časopis za more i pomorstvo, 69(2), pp. 77–83. Available at: https://doi.org/10.17818/NM/2022/2.1

Madi, M., Rafi, R., Asyidiqi, M.M., Hasbiyalloh, H. and Ronaldo, A. (2021a) 'Studi Eksperimen Model Water Flow Deflector untuk Meningkatkan Performa Turbin Arus Laut Tipe Vertikal pada Kecepatan Arus Rendah', Wave: Jurnal Ilmiah Teknologi Maritim, 15(2), pp. 85–90. Available at: https://ejournal.brin.go.id/jurnalwave/article/view/2306

Madi, M., Rahmawati, S., Satrio, D., Tuswan, T. and Ismail, A. (2024b) 'Experimental Study on the Effect of Single Flow Disturber on the Performance of the Straight-Bladed Hydrokinetic Turbine at Low Current Speed', Pomorstvo, 38(1), pp. 43–54. Available at: https://doi.org/10.31217/p.38.1.4

Madi, M., Tuswan, T., Arirohman, I.D. and Ismail, A. (2021b) 'Comparative analysis of taper and taperless blade design for ocean wind turbines in Ciheras coastline, West Java', Kapal: Jurnal Ilmu Pengetahuan dan Teknologi Kelautan, 18(1), pp. 8–17. Available at: https://doi.org/10.14710/kapal.v18i1.32486

Madi, Sasono, M.E.N., Hadiwidodo, Y.S. and Sujiatanti, S.H. (2019, August) 'Application of Savonius turbine behind the propeller as energy source of fishing vessel in Indonesia', in IOP Conference Series: Materials Science and Engineering, 588(1), p. 012046. Available at: https://doi.org/10.1088/1757-899X/588/1/012046

Madi (2020) Experimental Study on Improving The Performance of Marine Current Power Generating Turbines for Indonesian Water Areas (in Indonesian language). Thesis. Institut Teknologi Sepuluh Nopember.

Madi, Rahmawati, S., Mukhtasor, Satrio, D. and Yasim, A. (2021c) ‘Variation Number of Blades for Performance Enhancement for Vertical Axis Current Turbine in Low Water Velocity in Indonesia’, in Proceedings of the 7th International Seminar on Ocean and Coastal Engineering, Environmental and Natural Disaster Management - ISOCEEN. SciTePress, pp. 47–53. Available at: https://doi.org/10.5220/0010047900470053

Marsh, P., Ranmuthugala, D., Penesis, I. and Thomas, G. (2015) ‘Three-dimensional numerical simulations of straight-bladed vertical axis tidal turbines investigating power output, torque ripple and mounting forces’, Renewable Energy, 83, pp. 67–77. Available at: https://doi.org/10.1016/j.renene.2015.04.014

Mehmood, N., Liang, Z. and Khan, J. (2012) ‘Diffuser augmented horizontal axis tidal current turbines’, Research Journal of Applied Sciences, Engineering and Technology, 4(18), pp. 3522–3532.

Mohamed, M.H. (2012) ‘Performance investigation of H-rotor Darrieus turbine with new airfoil shapes’, Energy, 47(1), pp. 522–530. Available at: https://doi.org/10.1016/j.energy.2012.08.044

Mukhtasor (2014) Introduction to Ocean Energy (in Indonesian language). Surabaya: ICEES Press.

Münch-Alligné, C., Schmid, J., Richard, S., Gaspoz, A., Brunner, N. and Hasmatuchi, V. (2018) ‘Experimental assessment of a new kinetic turbine performance for artificial channels’, Water, 10(3), p. 311. Available at: https://doi.org/10.3390/w10030311

Nugraha, R.B.A., Erwandi, E. and Syahputra, H. (2018) ‘The Analysis of Tidal Current in Suramadu Bridge Pier for Marine Power Generation Test Site’, Jurnal Segara, 14(2), pp. 69–78.

Patel, V., Eldho, T.I. and Prabhu, S.V. (2017) ‘Experimental investigations on Darrieus straight blade turbine for tidal current application and parametric optimization for hydro farm arrangement’, International Journal of Marine Energy, 17, pp. 110–135. Available at: https://doi.org/10.1016/j.ijome.2017.01.007

Purba, N.P., Kelvin, J., Sandro, R., Gibran, S., Permata, R.A., Maulida, F. and Martasuganda, M.K. (2015) ‘Suitable locations of ocean renewable energy (ORE) in Indonesia region–GIS approached’, Energy Procedia, 65, pp. 230–238. Available at: https://doi.org/10.1016/j.egypro.2015.01.035

Sanvito, A.G., Dossena, V. and Persico, G. (2021) ‘Formulation, validation, and application of a novel 3D BEM tool for vertical axis wind turbines of general shape and size’, Applied Sciences, 11(13), p. 5874. Available at: https://doi.org/10.3390/app11135874

Sasmita, A.F., Arini, N.R. and Satrio, D. (2023, August) ‘Numerical Analysis of Vertical Axis Tidal Turbine: A Comparison of Darrieus and Gorlov Type’, in 2023 International Electronics Symposium (IES), pp. 26–31. IEEE. Available at: https://doi.org/10.1109/IES59143.2023.10242399

Satrio, D., Utama, I.K.A.P. and Mukhtasor (2016) ‘Vertical Axis Tidal Current Turbine: Advantages and Challenges Review’, International Society of Ocean, Mechanical and Aerospace Scientists and Engineers, 7 November, pp. 64–71.

Satrio (2019) Numerical and Experimental Study of Vertical Axis Ocean Current Turbine Performance (in Indonesian language). Doctoral Dissertation. Institut Teknologi Sepuluh Nopember.

Satrio, D. and Utama, I.K.A.P. (2021) ‘Experimental investigation into the improvement of self-starting capability of vertical-axis tidal current turbine’, Energy Reports, 7, pp. 4587–4594. Available at: https://doi.org/10.1016/j.egyr.2021.07.027

Satrio, D., Muhammad, F.Y., Mukhtasor, Rahmawati, S., Junianto, S. and Musabikha, S. (2022a) ‘Numerical simulation of cross-flow Savonius turbine for locations with low current velocity in Indonesia’, Journal of the Brazilian Society of Mechanical Sciences and Engineering, 44(8), p. 315. Available at: https://doi.org/10.1007/s40430-022-03620-w

Satrio, D., Suntoyo and Ramadhan, L.I. (2022b) ‘The advantage of flow disturbance for vertical-axis turbine in low current velocity’, Sustainable Energy Technologies and Assessments, 49, p. 101692. Available at: https://doi.org/10.1016/j.seta.2021.101692

Satrio, D., Albatinusa, F., Junianto, S., Musabikha, S., Madi, M. and Setyawan, F.O. (2023a, May) ‘Effect of Positioning a Circular Flow Disturbance in Front of the Darrieus Turbine’, in IOP Conference Series: Earth and Environmental Science, 1166(1), p. 012019. Available at: https://doi.org/10.1088/1755-1315/1166/1/012019

Satrio, D., Albatinusa, F. and Hakim, M.L. (2023b) ‘The Benefit Using a Circular Flow Disturbance on the Darrieus Turbine Performance’, International Journal on Engineering Applications, 11(1). Available at: https://doi.org/10.15866/irea.v11i1.22434

Satrio, D., Widyawan, H.B., Ramadhani, M.A. and Muharja, M. (2024) ‘Effects of the distance ratio of circular flow disturbance on vertical-axis turbine performance: An experimental and numerical study’, Sustainable Energy Technologies and Assessments, 63, p. 103635. Available at: https://doi.org/10.1016/j.seta.2024.103635

Satrio, D., Basunjaya, A., Wardhana, W., Hashim, F.E., Mubarok, M.A., Farid, M., Muharja, M., Ahsan, M., Hakam, A. and Madi (2025) ‘Technical feasibility of implementing heaving device wave energy converter: a case study in Mentawai Waters, Indonesia’, Marine Systems & Ocean Technology, 20(1), p. 4. Available at: https://doi.org/10.1007/s40868-024-00151-y

Scholz, D. (2022) ‘Calculating the Speed Ratio of Wind Turbines with General Cone and Axis Angle for the Unsteady Blade Element Momentum Theory (UBEMT)’. Available at: https://doi.org/10.20944/preprints202208.0228.v1

Shiono, M., Suzuki, K. and Kiho, S. (2002, May) ‘Output characteristics of Darrieus water turbine with helical blades for tidal current generations’, in ISOPE International Ocean and Polar Engineering Conference, pp. ISOPE-I.

Talukdar, P.K., Kulkarni, V. and Saha, U.K. (2018) 'Field-testing of model helical-bladed hydrokinetic turbines for small-scale power generation', Renewable Energy, 127, pp. 158–167. Available at: https://doi.org/10.1016/j.renene.2018.04.052

Utama, I.K.A.P., Satrio, D., Mukhtasor, Atlar, M., Shi, W., Hantoro, R. and Thomas, G. (2020) 'Numerical simulation of foil with leading-edge tubercle for vertical-axis tidal-current turbine', Journal of Mechanical Engineering and Sciences, 14(3), pp. 6982–6992. Available at: https://doi.org/10.15282/jmes.14.3.2020.02.0547

Winchester, J. and Quayle, S. (2011) 'Torque ripple and power in a variable pitch vertical axis tidal turbine', in The 9th European Wave and Tidal Energy Conference, Southampton, UK.

Yahya, N.Y. and Satrio, D. (2023, June) 'A Review of Technology Development and Numerical Model Equation for Ocean Current Energy', in IOP Conference Series: Earth and Environmental Science, 1198(1), p. 012019. Available at: https://doi.org/10.1088/1755-1315/1198/1/012019

Zaidi, S., Abbas, M.K., Saleem, S., Khan, B.M. and Haider, S. (2021, January) 'Renewable tidal power generation significance & challenges', in 2021 International Bhurban Conference on Applied Sciences and Technologies (IBCAST), pp. 1–6. IEEE. Available at: https://doi.org/10.1109/IBCAST51254.2021.9393280

TABLE OF ABBREVIATIONS

Abbreviations	Definitions
CoFD	Convergent Flow Disturbances
VAT	Vertical Axis Turbine
TSR	Tip Speed Ratio
Rpm	Revolutions per minute
N	Number of blades
S	Blade span (m)
D	Turbine diameter (m)
R	Turbine radius (m)
D	Shaft diameter (m)
AR	Aspect ratio
C	Chord length (m)
$\boldsymbol{\omega}$	Angular velocity (1/rad)
$\boldsymbol{V}$	Current speed (m/s)
$\boldsymbol{T}$	Torque (N.m)
$\boldsymbol{C_t}$	Torque coefficient
$\boldsymbol{M}$	Mass of the load (kg)
$\boldsymbol{g}$	Gravitational acceleration (m/s2)
$\boldsymbol{r}$	Torque arm (m)
$\boldsymbol{p}$	Density (kg/m3)
$\boldsymbol{A}$	Turbine area (m2)
$\boldsymbol{P_t}$	Mechanical power (watt)
$\boldsymbol{P_k}$	Kinetic power (watt)
$\boldsymbol{C_p}$	Power coefficient
$\boldsymbol{\upsilon}$	Circumferential speed
$\boldsymbol{\nu}$	Rotational speed (1/s)